Process Safety and Environmental Protection 188 (2024) 86–95

Contents lists available at ScienceDirect

Process Safety and Environmental Protection

journal homepage: www.journals.elsevier.com/process-safety-and-environmental-protection

Degradation of diethyl phthalate by photolysis of hydrogen peroxide electrogenerated using a Printex L6 carbon modified with Benzophenone cathode in an improved tangential flow cell

Taynara Oliveira Silva [a,b,*], Géssica de Oliveira Santiago Santos [a,b], Renata Colombo [c], Marcos Roberto de Vasconcelos Lanza [a,**], Manuel Andrés Rodrigo Rodrigo [b,**]

[a] São Carlos Institute of Chemistry, University of São Paulo (USP), 400, São Carlos, SP 13566-590, Brazil
[b] Department of Chemical Engineering, Universidad de Castilla-La Mancha, Ciudad Real 13071, Spain
[c] School of Arts, Sciences and Humanities, University of São Paulo, São Paulo, SP 03828-000, Brazil

ARTICLE INFO

Keywords:
Electrosynthesis
Hydrogen peroxide
Advanced oxidation processes
Gas diffusion electrode
Phthalates degradation

ABSTRACT

In this work, a gas diffusion electrode (GDE) made of Printex L6 carbon modified with 2.0 % w/w of benzophenone-3,3′,4,4′-tetracarboxylic dianhydride (PL6C/BTDA 2 %) was employed as cathode in a new 3D printed electrochemical cell with tangential flow. With this configuration, the performance of the technology was evaluated for hydrogen peroxide (H_2O_2) electrogeneration and remediation of aqueous wastes contaminated with diethyl phthalate (DEP) using different H_2O_2-based advanced oxidation processes (AOPs). The electrogeneration study was carried out varying the current density applied to the system, and it was found that 50 mA cm^{-2} was the best performing value, resulting in remarkable Faradaic efficiencies of nearly 100 %. This led to the production of higher amounts of H_2O_2 (442.5 mg L^{-1}) in 90 minutes at an acceptable energy consumption (8.5 kWh kg^{-1}) compared to values reported in the literature. Based on these findings, H_2O_2-based AOPs were employed to investigate the removal of DEP in cathodic compartment, including mediated electrochemical degradation with electrogenerated H_2O_2 (e-H_2O_2) and the integration of this technology with ultraviolet-C (UVC) photolysis (e-H_2O_2/UVC). The integrated e-H_2O_2/UVC obtained the best performance compared to single photolysis and e-H_2O_2, leading to the total elimination of DEP (90 μmol L^{-1}) within only 30 min of treatment, reaching the highest kinetic rate constant (0.3 min^{-1}). Fifteen by-products, generated through oxidation processes studied, were successfully identified by LC-MS/MS, enabling the proposal of the degradation mechanism of DEP.

1. Introduction

Interest in hydrogen peroxide (H_2O_2) production has surged owing to its versatile applications across various industries, notably in textiles and cosmetics, as well as in bacterial and viral disinfection and waste remediation processes. Indeed, it serves as a primary component in numerous advanced oxidation processes (AOPs), encompassing a range of electrochemical advanced oxidation processes (EAOPs), where it is generated electrolytically *in situ*. In addition to its high reduction potential ($E^\circ = +1.77$ V vs SHE), H_2O_2 can be activated in the presence of UVC irradiation to hydroxyl radical (•OH) ($E^\circ = +2.80$ V vs SHE)(De Araújo et al., 2016; Lima et al., 2020; Oturan and Aaron, 2014; Y. Song et al., 2016). This radical has been documented in the literature as being highly effective in the elimination of aqueous contaminants, even at low concentrations, including recalcitrant compounds that remain unresolved through conventional water treatment methods (Brillas, 2014; Cordeiro-Junior et al., 2022b). A notable example of such pollutants is phthalates, a class of plasticizers. Diethyl phthalate (DEP), among others, is recognized as posing significant health risks to both humans and animals. Phthalates function as endocrine-disrupting micropollutants capable of adversely perturbing the endocrine systems of living organisms. (Fromme et al., 2002; Heudorf et al., 2007; Van Wezel

* Corresponding author at: São Carlos Institute of Chemistry, University of São Paulo (USP), 400, São Carlos, SP 13566-590, Brazil.
** Corresponding authors.
E-mail addresses: taynaraos1994@alumni.usp.br (T. Oliveira Silva), marcoslanza@usp.br (M.R. de Vasconcelos Lanza), manuel.rodrigo@uclm.es (M.A. Rodrigo Rodrigo).

https://doi.org/10.1016/j.psep.2024.05.092
Received 8 February 2024; Received in revised form 14 May 2024; Accepted 20 May 2024
Available online 22 May 2024

et al., 2000).

To produce H_2O_2 in the context of alternative water treatment technologies, electrochemical synthesis stands as a favorable approach (Xia et al., 2019). This is primarily because H_2O_2 can be generated *in situ* directly from the water undergoing treatment, hindering the necessity for the storage or transportation of this chemical compound·H_2O_2 can be produced through the cathodic process of the oxygen reduction reaction (ORR) when it proceeds via the two-electron ($2e^-$) pathway, as depicted in Eq. 1. In contrast, when the ORR follows the four-electron ($4e^-$) pathway, water (H_2O) is the resulting product. Hence, in the search of efficient processes, it is imperative to use catalytic materials that do not only exhibit high activity for the complete ORR but only selectivity for the $2e^-$ pathway (Kulkarni et al., 2018; Ma et al., 2019; Zhou et al., 2019).

$$O_2 + 2H^+ + 2e^- \rightarrow H_2O_2 \quad (1)$$

$$O_2 + 4H^+ + 4e^- \rightarrow 2H_2O \quad (2)$$

Carbon-based materials, particularly amorphous carbons like Printex L6 carbon (PL6C), exhibit notable selectivity for $2e^-$ pathway in the ORR (Bu et al., 2022). This selectivity is a result of a number of variables, their favorable electrical conductivity, the presence of functional groups within their structure and on their surface, and their important surface area (Cordeiro-Junior et al., 2022a, 2020a). An advantageous characteristic of utilizing carbon, such as PL6C, as a catalytic matrix lies in its modifiability with various compounds, which can enhance its performance in the production of hydrogen peroxide (H_2O_2) (Cordeiro-Junior et al., 2020b; Kronka et al., 2023).

In this regard, numerous compounds, ranging from metal oxides to complexes and organic substances, have been subjected to investigation as potential catalytic modifiers (Carneiro et al., 2017; Moreira et al., 2019; Valim et al., 2021). Within the realm of organic compounds, the incorporation of Benzophenone-3,3′,4,4′-tetracarboxylic dianhydride (BTDA) exhibited notable enhancements in selectivity and efficiency concerning the electrogeneration of H_2O_2 when coupled with PL6C (Michielli and Elving, 1968; Silva et al., 2022). This favorable outcome can be attributed to the structural characteristics of BTDA, which encompasses multiple oxygenated functional groups. These groups, in synergy, contribute significantly to augmenting the electrosynthesis of the desired oxidant (Escobar et al., 2010; Hou and Sun, 2013; Yegorov et al., 2016).

Beyond the selection of a catalytic material, it is important to investigate the operational parameters governing the effective generation of substantial quantities of H_2O_2. One viable approach involves the incorporation of these materials into gas diffusion electrodes (GDE) (Barros et al., 2015; Wang et al., 2021; Zhu et al., 2019). These electrodes are characterized by a tripartite interface (gas-solid-liquid), enabling the direct delivery of O_2 gas, the principal reagent in the ORR, to the reaction surface. This hinders the necessity for dissolving O_2 gas in the solution, which is non efficient because of the low solubility of O_2 in water and that only can be improved operating at high pressures and low temperatures (Lima et al., 2020; Muddemann et al., 2020).

The configuration of the electrochemical cell is another pivotal factor that significantly influences the feasibility of implementing this technology at a full-scale level (da Costa et al., 2021; Silva et al., 2023; Yu et al., 2014), being specially important the fluid dynamics attained, because it may help to reach higher efficiencies.

This study endeavors to achieve optimal current efficiency in the electrogeneration of H_2O_2 through the utilization of a newly developed electrochemical cell, this cell, fabricated via 3D printing to enable tangential flow, specifically engineered for this purpose and features a pioneering GDE comprised of PL6C modified with 2 % BTDA. In this electrochemical cell, a PEM-type membrane will be used not only expected to serve as separator (avoiding the H_2O_2 to be consumed by scavengers) but also to allow only the passage of H^+ which also will contribute to greater efficiencies in H_2O_2 electrogeneration as has been already reported in a previous work by our research group (Silva et al., 2023) The primary objective is the complete removal of DEP employing various AOPs, encompassing mediated electrochemical degradation utilizing electrogenerated H_2O_2 (e-H_2O_2) and its integration with UVC photolysis (e-H_2O_2/UVC). The attainment of successful outcomes holds significant promise in paving the way for more efficient electrosynthesis of H_2O_2 and advancements in wastewater treatment methodologies.

2. Material and methods

2.1. Material

For the manufacture of GDE the carbon (carbon black Printex® L6 – PL6C) was purchased from Evonik Brazil ltd., benzophenone-3,3',4,4'-tetracarboxylic dianhydride ($C_{17}H_6O_7$ – BTDA) with a purity of > 98 % produced by Aldrich, the carbon cloth from Zoltek, (model PX30), and the poly(tetrafluoroethylene)-(PTFE) was obtained from Sealflon. Sodium sulfate (Na_2SO_4, ≥99 %) purchased from Merck was used in the preparation of electrolyte solutions used for H_2O_2 electrogeneration and for degradation experiments. Diethyl phthalate ($C_{12}H_{14}O_4$ – DEP) with a purity > 99.5 % was obtained from Sigma Aldrich. A Proton exchange membrane (PEM), Neosepta CMX, obtained from Astom Corporation was used to separate the anodic and cathodic compartment in the double-compartment cell configuration. Acetonitrile multisolvent (HPLC grade) was acquired from Scharlau, sulfuric acid (H_2SO_4) with a purity of >98 %, titanium (IV) oxysulfate solution ($TiOSO_4$ ~ 1.9–2.1 %) and potassium bromide (KBr) purity of >99 % (FTIR grade) were acquired from Sigma Aldrich and used in the analytical analysis. Ultrapure water (resistivity ≥18.2 MΩ cm) was used in all stages of the research, (Millipore Milli-Q system).

2.2. Gas diffusion electrode production

The manufacture of the GDE is based on the procedures described elsewhere (Cordeiro-Junior et al., 2022a; Silva et al., 2022). A catalytic mass consisting of PL6C and/or PL6C/BTDA 2 % w/w is mixed in a proportion of % w/w vigorously with PTFE in 500 mL ultrapure water. Then, it is vacuum filtered, and 2 g of the material are deposited onto a carbon cloth surface (120 cm^2) and double-plate hydraulic press (from SOLAB, Brazil) with heating accoupled with a termocouple (2 tons for 25 min at 210°C of temperature). Afterward, the cloth was cut into 20 cm^2 circular shape area to fit the 3-D printed cell compartment.

2.3. Characterization of the gas diffusion electrode

To determine the contact angles of the modified and unmodified GDE was used an angle meter from Attension Theta. Contact angle measurements were recorded by the angle formed by the contact of a drop of ultrapure water (3.0 μL) on the surface of the electrode of interest. Using a scanning electron microscope (JEOL model JSM 6510 V), scanning electron microscopy (SEM) was used to analyze the surface morphology of the GDE.

Fourier transform infrared spectroscopy (FTIR) was carried out on both materials (modified and unmodified), using the tablet method in which 1 mg of the material of interest was macerated with 100 mg of KBr until it was homogeneous, and this material was pressed to form a tablet. The spectra were obtained in a wave range from 500 to 4000 cm^{-1} using Tensor 27 from Bruker.

To determine the mass composition of the materials, CHNSO elemental analysis was carried out using Thermo Scientific FlashSmart and the PL6C and PL6C/BTDA 2 % materials were analyzed at a temperature of 950 °C for 720 seconds run time, the oxygen values were obtained by difference ("O*").

2.4. Experimental setup and operation procedure

To produce hydrogen peroxide, a tangential-flow electrochemical cell was mechanically designed using Fusion 360. This reactor consisted of four frame pieces specifically designed to hold the GDE allowing gas to enter and the possibility of using a membrane dividing the compartments, and they were made of resin (photopolymer Grey Pro - From Formlabs) by a 3D printer (Form 3+ Stereolithography – from Formlabs), and integrated mechanically with seal gaskets and screws, the resin was chosen carefully to not suffer attack by the chemicals and the oxidant species generated in it. A GDE (PL6C and PL6C/BTDA 2 %) cathode and a dimensionally stable anode (DSA®-Cl_2) anode from DeNora S.P.A. in Brazil, both sizing 20 cm^2, were integrated in the cell, as well as a cation exchange membrane that separate the anodic and cathodic compartments. Electrodes were connected to a power supply ES030–10 (15 V/10 A) from Delta Elektronica. Production of hydrogen peroxide was made under galvanostatic conditions and current densities were modified in the different tests from 25 to 200 mA cm^{-2}. Both compartments of the cell were hydraulically connected to reservoir tanks (with a capacity of 2.0 L) that contained 1.0 L of electrolyte each (Na_2SO_4 0.5 mol L^{-1}) with pH 2.5, adjusted with H_2SO_4. The electrolytes were recirculated between the reservoir tanks and the electronic compartments by two peristaltic pumps (Percom N-M II from JP Selecta group) with a flow rate of 250 mL min^{-1}. Temperature of the electrolytes was kept with a thermostatic bath fixed at 25°C (Tectron-200 27 from JP Selecta group) (Silva et al., 2023). The flowrate of O_2 fed to the GDE was 50.0 mL min^{-1}. The design of developed electrochemical reactor is shown in the Fig. SM1 in the supplementary material of the present work.

The same system used for the electrogeneration of H_2O_2 was used to treat the diethyl phthalate synthetic wastes (replacing the electrolyte used for hydrogen peroxide production by a solution with an initial concentration of DEP 20 mg L^{-1} (90 μmol L^{-1})).

Several technologies were tested:

- Mediated electrochemical degradation with the cathodically produced hydrogen peroxide (e-H_2O_2), in which it is evaluated the oxidation of DEP with hydrogen peroxide produced on the GDE, when this electrode is fed with a stream of O_2,
- Photolysis with a 254 nm ultraviolet C light (UVC) of 9 W in which the electrodes of the reactor were not connected to the power supply and only UVC light was irradiated to the aqueous waste, while it was flowed through the hydraulic circuit of the cell,
- Integrated process (e-H_2O_2/UVC) in which the combined effect of hydrogen peroxide produced electrolytically and UVC is evaluated.

In the photolysis and e-H_2O_2/UVC the lamp is immersed in the reservoir tank. A fixed current density of 50 mA cm^{-2} was applied in the e-H_2O_2 and e-H_2O_2/UVC degradation systems and was chosen after H_2O_2 electrogeneration optimization study.

2.5. Analytical procedures

To measure the H_2O_2 in solution, titanium (IV) oxysulfate solution was utilized as an indicator reagent (at $\lambda = 408$ nm), The indicator reagent forms a complex with H_2O_2, enabling the quantification through spectroscopic analysis (Chai et al., 2004), using a UV-Vis spectroscopy (Shimadzu UV- 1700 Spectrophotometer)(Moratalla et al., 2021). The evolution of the DEP concentration was followed using high-performance liquid chromatography (HPLC) with a UV-DAD (Agilent 1100 Series) detector was used. The stationary phase was a Phenomenez Kinetex C18 column 5 μm particle size (150 mm × 4.6 mm), and the mobile phase consisted of a mixture of acetonitrile and 10 % formic acid in water (70:30; v/v), in isocratic elution mode (at 0.8 mL min^{-1}). At a temperature of 30°C and an injection volume of 20 μL, DEP was detected at 228 nm. Considering the following: The relative percentage decay of DEP was computed as [DEP]/[DEP]0 × 100 %, where [DEP] and [DEP]0 are the values at a predetermined interval and the start of the experiment, respectively. The analysis involved filtering the obtained materials using a Chromafil syringe filter (0.45 μm).

Carboxylic acids intermediates were monitored by HPLC (Shimadzu – UFLC 20) using a HiplexH reversed- column (7.7 mm × 300 mm) as stationary phase and the mobile phase consisted of 0.1 M H_2SO_4 at flow rate of 0.6 mL min^{-1}, with detection at 210 nm. The temperature of the column was set to 60 °C. The acid intermediates were identified by comparison with retention time of standard solutions.

The degradation by-products and degradation pathway were determined using a liquid chromatograph system (Prominence LC 20AT) coupled to a triple quadrupole mass spectrometer (LC-MS/MS 8030), both acquired from Shimadzu (Kyoto, Japan). Chromatographic separation was achieved using a Shim-pack ODS II column (dimensions: 100 mm × 3.0 mm × 2.2 μm) with a flow rate of 0.6 mL min^{-1}. The mobile phase was a combination of 0.1 % formic acid in water (A) and acetonitrile (B) and the elution was performed in gradient mode: 0 −5 min: 10–100 % B; 5–8 min: 100 % B; 8–10 min: 100–10 % B). The analysis was performed with electrospray ionization (ESI) interface in positive ionization mode with a scan range of m/z between 50 and 500. The desolvation gas (N_2) flow rate was set at 1 L min^{-1}, and the temperature of desolvation and ion source block was maintained at 250°C and 400°C, respectively. Mass spectra were obtained over a capillary voltage of 4 kV and collision energy of 35 eV.

3. Results and discussion

3.1. Characterization of the gas diffusion electrode materials

Fig. 1 illustrates the images utilized for calculating the hydrophilicity of the GDE surface, determined by the contact angle between a water droplet and the GDE surface. Additionally, SEM photos of the GDE surface are depicted. It is well-established that an efficient GDE must facilitate the formation of triple phase boundaries (solid-liquid-gas). This requirement necessitates adequate hydrophilicity to allow for liquid permeation through the electrode surface while maintaining suitable hydrophobicity to enable gas flow along preferential paths to the active sites. This balance is typically achieved by a PL6C GDE, elucidating its commendable performance. (Giomo et al., 2008; Wang et al., 2021). As observed, the average contact angle values for the PL6C GDE and the PL6C/BTDA 2 % GDE were 124.29° and 123.79°, respectively. This indicates that the addition of the modifier BTDA does not significantly influence the hydrophilicity of the modified GDE. However, it introduces new functional groups that could potentially enhance the catalytic behavior of the ORR.

Concerning the SEM images, it is evident that the diffusion layer, situated on a carbon fabric substrate, demonstrates successful deposition of the catalytic layer. This results in the formation of a thin layer characterized by minimal surface fissures. (Cordeiro-Junior et al., 2022a, 2022b; Marques Cordeiro-Junior et al., 2022). These electrodes commonly exhibit a pattern characterized by shallow cracks, which can be attributed to the inherent flexibility of the carbon fabric within the diffusion layer, thereby facilitating the development of these small fissures. Importantly, a thorough analysis of the electrode surface revealed an absence of regions lacking the catalytic layer. This outcome indicates a strong adherence of the catalytic layer to the carbon fabric, a notable advantage attained through the utilization of the high-pressure method during the preparation of the GDE at elevated temperatures. (Moreira et al., 2019).

To characterize the surface functional groups of the materials, the Fourier transform infrared (FTIR) spectrum was analyzed (Fig. SM2). According to the spectra, the materials exhibit several oxygenated groups within their structure, including C-OH (1357 cm^{-1}), C═O (1715 cm^{-1}), N═O (1446 cm^{-1}), and O-H (3665 cm^{-1}), along with C═C

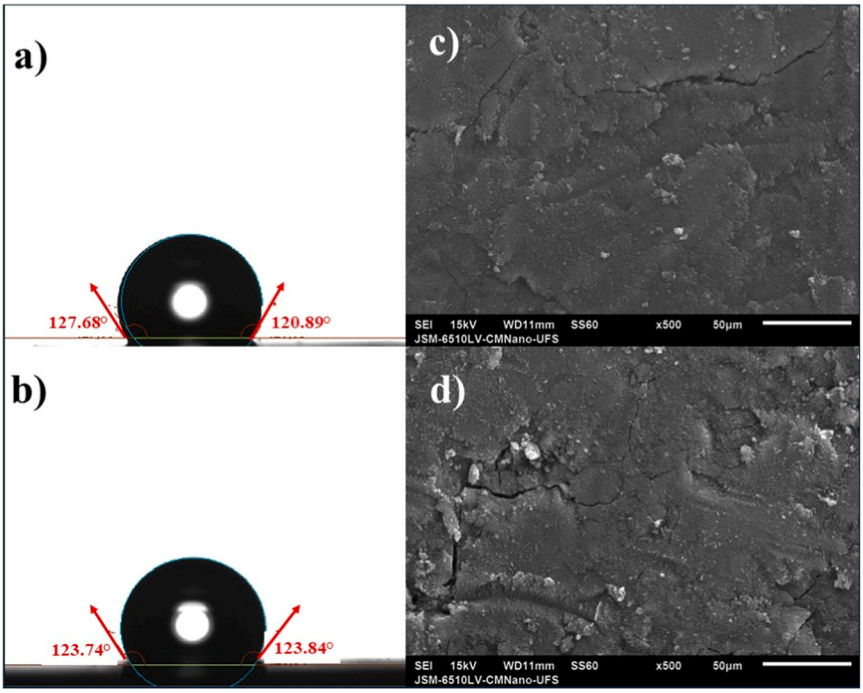

Fig. 1. Contact angles of the ultrapure water droplets on the GDE: a) PL6C. b) PL6C/BTDA 2 %. SEM images of the GDEs: c) PL6C. d) PL6C/BTDA 2 %.

(1547 cm^{-1}), which is typical of carbonaceous materials (Adinaveen et al., 2013; Posher, 1983). However, due to the minor 2 % modification and the composition of BTDA and PL6C (comprising carbon, oxygen, and hydrogen) it is very difficult to discern differences between the two materials. Consequently, elemental analysis was conducted on the materials, depicted in Fig. SM3, reveals a higher oxygen content in the 9.5 % modified material compared to the 6.2 % unmodified material. This discrepancy can be attributed to the presence of BTDA, which contains numerous oxygenated groups within its structure, thereby causing an anticipated reduction in the carbon content (Hong et al., 2021; Quan et al., 2018).

3.2. Electrogeneration of H_2O_2

In order to study the performance of GDE (with and without BTDA in its composition) in the H_2O_2 electrogeneration, several electrolysis were conducted with current densities ranging from 25 to 200 mA cm^{-2}. Fig. 2 shows the production of H_2O_2 in each test and the fitting of experimental data to a straight line, which corresponds to a zero-order kinetic model, whose integration in a discontinuously operated electrochemical cell corresponds to Eq. 1, where the concentration of H_2O_2 at time t is expressed by $C_{H2O2}(t)$ and k_{H2O2} is the zero-order kinetic constant (s^{-1}) (Silva et al., 2022).

$$C_{H2O2(t)} = -k_{H2O2}\, t \tag{3}$$

Regardless of the GDE composition, increases in current density result in higher production of H_2O_2. Also, it is important to comment that a linear behavior for H_2O_2 production is observed, on the contrary to the well-documented plateau that appears in non-divided electrochemical cells (Cordeiro-Junior et al., 2022a). This linear behavior can be explained in terms of the prevention of the direct oxidation of H_2O_2 on the surface of the anode as well as because of the prevention of the action of scavengers species generated on the anode, because of the use of the membrane. (Silva et al., 2022). However, by comparing the modified and unmodified GDE, it can be observed a positive effect of the addition of BTDA that low current densities: 50 and 100 mA cm^{-2}

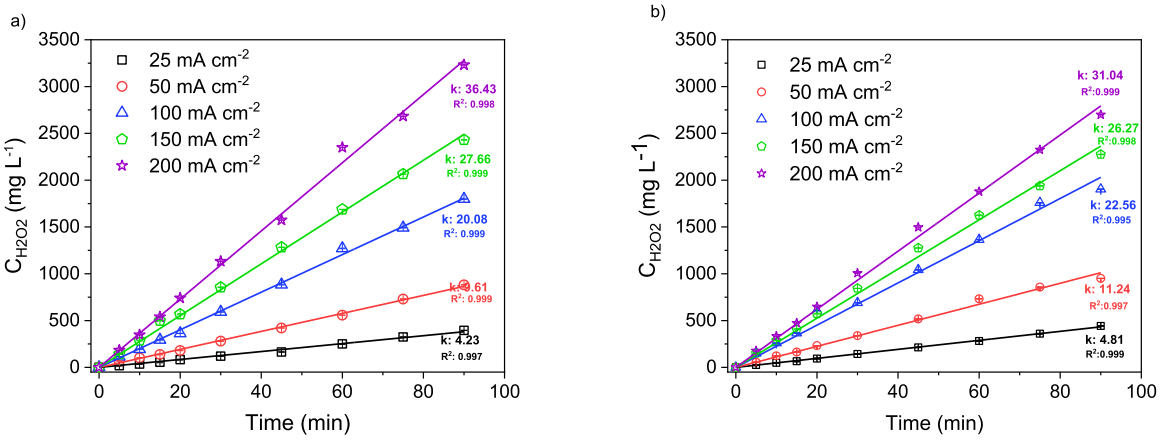

Fig. 2. Concentration of H_2O_2 electrogenerated under different current densities for 90 min in a divided cell and apparent kinetic constants (k_{H2O2}). a) GDE PL6C and b) GDE PL6C/BTDA 2 %. Electrolyte Na_2SO_4 0.5 mol L^{-1}, 1 L, flow rate 250 mL min^{-1}, pH 2.5 adjusted with H_2SO_4.

achieved concentrations of H_2O_2 of 442.5 and 951.5 mg L^{-1}, respectively, while the unmodified GDE demonstrated H_2O_2 concentrations of 395.6 and 881.2 mg L^{-1} for equivalent current densities. However, for higher current densities (above 150 mA cm^{-2}), this relationship is reversed, with the unmodified GDE registering higher H_2O_2 values compared to the GDE containing the organic modifier. Selectivity for ORR via 2 e- is only displayed by the PL6C/BTDA 2 % at specific current density values: It is plausible that an overpotential may induce a loss of selectivity in the material when the applied electric current surpasses this threshold. Consequently, the reaction may proceed via $4e^-$, yielding H_2O instead of H_2O_2. This phenomenon has been previously documented in the scientific literature (Silva et al., 2022).

In addition, it is worth noting that the material under investigation in this study demonstrates a higher k_{H2O2} value in comparison to values documented in the literature. For example, Moreira et al. (2019) achieved a k_{H2O2} value of 24.10 mg L^{-1} min^{-1} for a current density of 150 mA cm^{-2}, while in the current study, a k_{H2O2} value of 26.27 mg L^{-1} min^{-1} was obtained at the same current density (Moreira et al., 2019). Silva et al. (2023) also conducted research with a PL6C GDE modified with 2 % BTDA, applying a current density of 50 mA cm^{-2}, and reported a k_{H2O2} value of approximately 3.00 mg L^{-1} min^{-1}(Silva et al., 2022). This value is notably lower than the corresponding value in the present study, which was as high as 11.24 mg L^{-1} min^{-1} at the same current density. This discrepancy can be attributed to the methodology employed in this study for the GDE, which involves the utilization of carbon fabric as a support for the catalytic material. This discrepancy can be attributed to the methodology employed in this study for the GDE, which involves the utilization of carbon fabric as a support for the catalytic material, this innovative approach enables the reduction of the proportion of PTFE while preserving the efficiency of H_2O_2 generation and ensuring the stability of the material assessed at harsh conditions as document in a previous study (Marques Cordeiro-Junior et al., 2022), another factor contributing to the higher levels of H_2O_2 production compared to the findings of Silva et al. (2023). is the positive influence of the novel type of electrochemical cell used, that has an efficiency performance because of the tangential flow produced inside the cell that, in turn, contributes to increase mass transfer importantly, as already been reported in an work that study the same principle of tangential flow (da Silva et al., 2023).

The effect of the BDTA addition is also seen in Fig. 3, which shows the Faradaic efficiencies (FE) and energy consumption (EC), calculated according to Eq. 2 and 3 respectively, where mH_2O_2 is the mass of H_2O_2 (in g) in Eq. 2 and mass of H_2O_2 (in kg) for Eq. 3, I is the applied current (in A), t is the time (in seconds) for Eq. 2 and time (in hours) for Eq. 3. Two (2) is the stoichiometric number of electrons involved in the process and F is the Faraday constant (96486 C mol^{-1}) for Eq. 2. *Ecell* corresponds to cell potential (in V) for Eq. 3 (Sánchez-Montes et al., 2023; Silva et al., 2022).

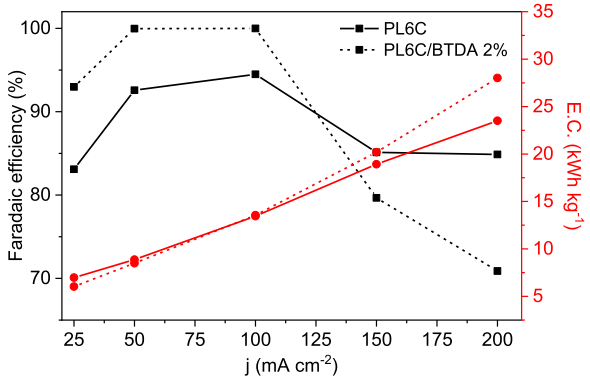

Fig. 3. Calculations of Faradaic efficiency and energy consumption for both electrodes PL6C and PL6C/BTDA 2 %.

$$FE(\%) = \frac{mH_2O_2}{mH_2O_2 theoretical} \times 100\% = \frac{mH_2O_2}{I \times \quad t \times 34/2F} \times 100\% \quad (4)$$

$$\text{EC (kWh kg}^{-1}) = \frac{E_{cell} \quad \times I \quad \times t}{mH_2O_2} \quad (5)$$

As expected according to the changes in the production, the faradaic efficiency increases from 25 to 100 mA cm^{-2} and reverts this trend at higher current densities, which support the change in the primary oxygen reduction reaction from the 2 to the 4 electron transfer mechanisms. In the first region the modified electrode is more efficient reaching FE of 99.99 % at current densities of 50 and 100 mA cm^{-2}, which are higher than those obtained by the bare PL6C GDE, which reached 94.48 % at 100 mA cm^{-2}. Regarding the energy efficiency, the situation is different because in this case the cell voltage increases importantly with the current density, making that energy consumption increases progressively with the increase in this parameter. Anyhow, operation at 50 mA cm^{-2} exhibits a suitable value with an energy consumption of 8.5 kWh kg^{-1} compared to 13.5 kWh kg^{-1} needed for operation at 100 mA cm^{-2} and because of that, it can be proposed as a very convenient choice for this process.

The better performance of BTDA-modified material when operated at the most efficient conditions with respect to the conventional GDE can be elucidated in terms of the direct involvement of BTDA in the reaction mechanisms for H_2O_2 formation, in turn associated with the capability to both oxidize and reduce the central oxygen within its molecular structure, thereby facilitating the direct production of H_2O_2, as illustrated in Fig. 4. This phenomenon has previously been documented in the literature for quinones and anthraquinones. Given the structural similarities between benzophenones and quinones, it is reasonable to anticipate that they may exhibit comparable behavior. Additionally, it is noteworthy that, aside from the direct influence of BTDA, a synergistic interaction should be occurring between the modifier and the carbon matrix. Owing to the presence of multiple oxygenated groups within the BTDA structure, its alterations in the electron density of the carbon matrix can be promoted. This modification results in the emergence of a larger number of active sites within the catalytic matrix (PL6C). These additional active sites account for the heightened generation of H_2O_2 and the concurrent increase in FE, the effect of increasing active sites was also evidenced by Xia et al. (2019) after chemical treatment of carbon black with nitric acid, adding more oxygenated groups to its surface (Xia et al., 2019).

These results underscore the remarkable effectiveness of the technology, wherein the utilization of GDE featuring an optimized catalytic material (PL6C/BTDA 2 %) led to the attainment of maximum FE, an unprecedented achievement in comparison to existing literature. Several pivotal factors were instrumental in achieving this maximum FE. First and foremost, the PL6C/BTDA 2 % material constituting the GDE exhibited high activity for the ORR and exceptional selectivity for the $2e^-$ reduction pathway. Moreover, it demonstrated synergistic behavior with the carbon matrix, enhancing H_2O_2 electrogeneration. A pivotal factor influencing the technology's performance is the configuration of the electrochemical cell, as previously emphasized, wherein the GDE is seamlessly integrated. In this setup, a proton exchange membrane separate the cathode and anode, resulting in increased current efficiency and higher quantities of electrogenerated H_2O_2, as previously reported (Silva et al., 2023). Lastly, the 3D printed electrochemical cell with tangential liquid flow plays a key role. A very recent study by our research groups demonstrated, by means of CFD modelling, that this configuration ensures thorough contact of the entire electrolyte with the electrode surface, eliminating dead volume and promoting high mass transport rates and turbulence (da Silva et al., 2023). The synergistic influence of all these factors enabled the generation of substantial quantities of H_2O_2 with maximum current efficiency.

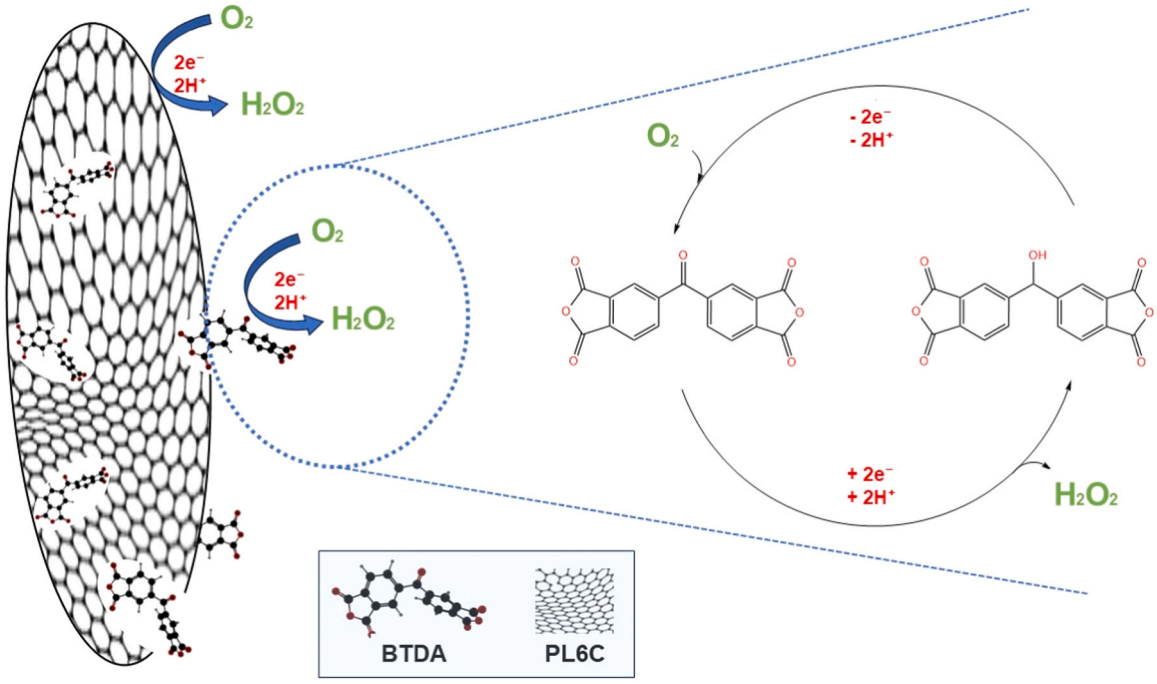

Fig. 4. Proposed reaction mechanism for electrogeneration of H_2O_2 with GDE PL6C/BTDA 2 %.

3.3. Degradation of diethyl phthalate

The GDE PL6C/BTDA 2 % was used in DEP degradation experiments at current density of 50 mA cm^{-2}, recirculating through the cathodic compartment of the electrochemical cell a synthetic wastewater containing this pollutant. The anodic compartment was fed with a solution containing the same electrolyte and no pollutants, because its characterization was not the target of this research, focused only on the cathodic compartment. The degradation of DEP by different process is shown in Fig. 5. It is worth highlighting that when employing the e-H_2O_2 and UVC technologies, a consistent degradation pattern for DEP was observed. These treatment technologies achieved a substantial reduction in DEP concentration, reaching values within the range 60–70 %, after treating the waste for 90 minutes. Previously, Xu et al. (2007) conducted research focused on the removal of DEP through the addition of H_2O_2 and the research findings revealed that, after a reaction duration of 3 hours, there was no discernible alteration in the initial concentration of DEP. This observation underscores the considerable inertness of DEP, indicating that it does not undergo degradation solely through the action of H_2O_2 (Xu et al., 2007; Yang et al., 2005). In a separate investigation conducted by Dong et al. (2016), it was evaluated the impact of electrochemical oxidation as a sole treatment method on the degradation of DEP (50 mg L^{-1}), and the study revealed that when applying a current density of 200 mA cm^{-2} a complete degradation of DEP was achieved within a 120 min. This outcome aligns with the findings of the current study, wherein it is substantiated that the degradation observed by e-H_2O_2 and this result may be associated to the activation of the hydrogen peroxide by means of other processes that takes place on the cell (Dong et al., 2016).

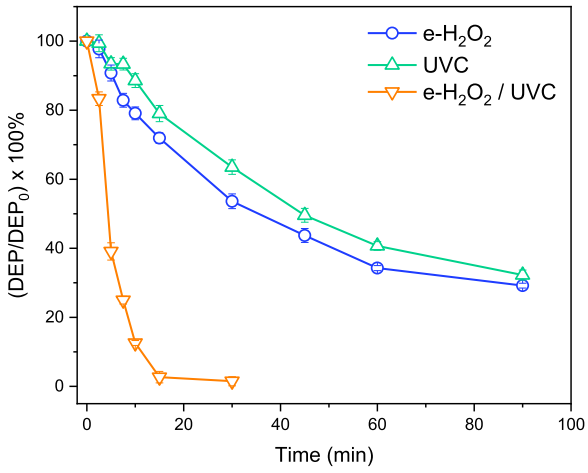

Fig. 5. Relative percentage of DEP degraded over time under various treatment procedures with GDE PL6C/BTDA 2 % and a 50 mA cm^{-2} density current applied. Electrolyte Na_2SO_4 0.5 mol L^{-1}, 1 L, flow rate 250 mL min^{-1}, pH 2.5.

Photodegradation exhibits a degradation pattern consistent with the previously discussed processes, resulting in the partial degradation of DEP in 90 minutes duration tests. This behavior can be attributed to the inertness of DEP, rendering it relatively resistant to UV irradiation. This observation agrees with prior findings in the literature, as reported by Medellin-Castillo et al. (2013). In that study, the application of UV light (15 W) for 180 minutes led to a partial degradation of approximately 70 %, equivalent to the reduction of initial 21.89 mg L^{-1} of DEP (Medellin-Castillo et al., 2013).

The oxidation of DEP molecule exhibited remarkable enhancement when the coupled approach of e-H_2O_2/UVC was employed. This hybrid treatment strategy achieved complete DEP elimination within a mere 30 min treatment duration. The significant enhancement observed in this treatment process can primarily be attributed to the •OH, generated through the activation of H_2O_2 under UVC irradiation, as delineated in Eq. 4 (Li et al., 2017; Sánchez-Montes et al., 2023; Y. Song et al., 2016).

$$H_2O_2 + h\nu \rightarrow \quad 2 \quad {}^{\bullet}OH \tag{6}$$

These •OH species selectively target the DEP molecule and its completely oxidation, causing its degradation, expected behavior according to the literature as it is a strong oxidant already consolidated in science (Chaplin, 2014; Jing and Chaplin, 2017; Wang and Xu, 2012; Xiao and Ouyang, 2009). Hence, among the investigated processes, the combined treatment approach that facilitates the generation of highly reactive and non-selective radicals (•OH) attains complete molecule

removal within a remarkably brief duration of 30 minutes.

To gain further insights into the process underlying the degradation of DEP, pseudo-first-order kinetic constants (k_{1st}) were calculated (by fitting experimental data) for the various treatment processes and are presented in Fig. 6a. The data reveal that, as anticipated, the k_{1st} values are notably similar for the e-H_2O_2 and UVC processes, with values of 3.94 and 3.67 $\times 10^{-2}$ min^{-1}, respectively. These findings align with the observed DEP degradation trends. In contrast, the e-H_2O_2/UVC process demonstrated a substantially higher rate constant, 30.0 $\times 10^{-2}$ min^{-1}, which exceeded the values attained when each individual treatment process was applied by a factor of more than sevenfold, clearly pointing out the existence of a synergistic behavior in the integration of both degradation technologies.

Song et al. (2016) found that applying the H_2O_2/UVC procedure at the start of the experiment resulted in a comparatively lower k_{1st} value (~ 4.0 $\times 10^{-2}$ min^{-1}) equivalent to DEP (45 μmol L^{-1}) removal as compared to the value observed in this investigation. (C. Song et al., 2016). The kinetics results are also superior to those studied by Medellin-Castillo et al. (2013), who also adding H_2O_2 at the beginning of the reaction and activating with UVC (H_2O_2/UVC) studied the degradation of DEP (40 mg L^{-1}) and found a k_{1st} value of 3.6 $\times 10^{-2}$ min^{-1} (Medellin-Castillo et al., 2013). The disparity noted in the k_{1st} values between the current study and previously reported works in the literature can be attributed to the continuous *in situ* electrogeneration of H_2O_2 facilitated by the GDE and, as well, to the performance of the 3D printed electrochemical cell. This setup ensures the constant availability of the oxidant, ready for activation throughout the entire experimental duration. It is important to consider that the GDE, utilizing PL6C/BTDA 2 %, efficiently generates substantial quantities of electrogenerated H_2O_2 and can supply quantities of •OH sufficient to sustain a robust degradation kinetics.

Eq. 5. provided below was employed for the purpose of assessing and comparing the treatment methods in relation to their electrical energy consumed per order of decrease of the pollutant concentration (E/EO), where E_{cell} is the cell potential in V, P_{lamp} is the power of the UVC lamp in W, 6.39 $\times 10^{-4}$ is a conversion factor (1 h/3600 s/0.4343), k_{1st} is the pseudo-first order rate constant in s^{-1}, and V is the volume in m^3. This approach allows for a comprehensive evaluation of the treatment methods with respect to their feasibility and efficiency in the oxidation of DEP, show in Fig. 6b (Silva et al., 2022).

$$E\Big/EO\left(kWhm^{-3}order^{-1}\right) = \frac{6.39x10^{-4}\quad (E_{cell}+P_{lamp})}{V\ x k_{1st}} \tag{7}$$

Once again, the superior performance of the combined e-H_2O_2/UVC process is clear. This process presents the lowest E/EO value, quantified at 2.17 kWh m^{-3} $order^{-1}$, while the individual processes showed significantly higher energy consumption, with values of 13.58 kWh m^{-3} $order^{-1}$ to e-H_2O_2 and 25.37 kWh m^{-3} $order^{-1}$ to UVC. The combined process stands out as the most advantageous among the studied methodologies. One of the key factors contributing to this superiority is its reduced energy requirement to achieve a one-order magnitude reduction of the pollutant DEP, underscoring its environmentally friendly character. It is significant to remember that E/EO values depend on a number of variables, such as the supporting electrolyte, hydrodynamic circumstances, applied electric current density, and starting contaminant concentration.

3.4. Proposal pathway of DEP degradation

By selecting the Selected Ion Monitoring (SIM) and Full Scan (range of *m/z* 50–500) modes, it was possible to determine the molecular ion of the DEP molecule ([M+H]+, *m/z* = 223) and its characteristic fragment at *m/z* 177 (Chingin et al., 2009; Farissi et al., 2023; Mansouri et al., 2019; Wu et al., 2019).

Fifteen DEP degradation products (DP1–DP15) were identified in the treatments processes (e-H_2O_2; UVC and e-H_2O_2/UVC). Chromatographic and mass spectrometry information for these degradation compounds is displayed in Table 1 and Fig. SM4. Based on the identified products, four transformation pathways of DEP were proposed (Fig. 7).

In Pathway I, the occurrence of self-coupling of phenoxy radicals and successive hydroxylation processes of DEP were suggested, leading to the formation of high-molecular-weight products DP1 (*m/z* 479), DP2 (*m/z* 495), and DP3 (*m/z* 499). The cross-coupling processes of DEP radicals have been described in the literature (Zhang et al., 2024). Degradation reactions of these high-molecular-weight compounds can also occur through the attack of •OH radicals, with the likely formation process for DP4 at *m/z* 391, DP5 at *m/z* 353, and DP6 at *m/z* 339. The formation of these intermediates occurred through the fragmentation of DP2 and/or DP3 with losses of moieties such as CH_4O, H_2O, C_2H_6O, and/or CH_4O_2. These coupling reactions which resulted in large molecular weight products, including dimeric photoproducts (combinations of the two parent compounds or of the parent compound and the product of UVC process) was only observed during UVC irradiation as observed in previous studies (Zhang et al., 2024).

A second mechanism for the formation of intermediates (Pathway II) was proposed by the continuous hydroxylation of the DEP molecule, leading to the formation of DP7 (*m/z* 253), DP8 (*m/z* 271), DP9 (*m/z* 301), DP10 (*m/z* 317), and DP11 (*m/z* 227).

Pathway III describes the oxidation of DEP, with DP12 at *m/z* 279 being the only intermediate formed by this route.

The attack of the hydroxyl radical on the DEP molecule, causing the breaking of C-C and C-O bonds, is proposed in Pathway IV. The loss of two methyl groups from DEP generated DP13 (*m/z* 195), the removal of a methoxy unit from DP13 gave rise to DP14 with *m/z* 165, and

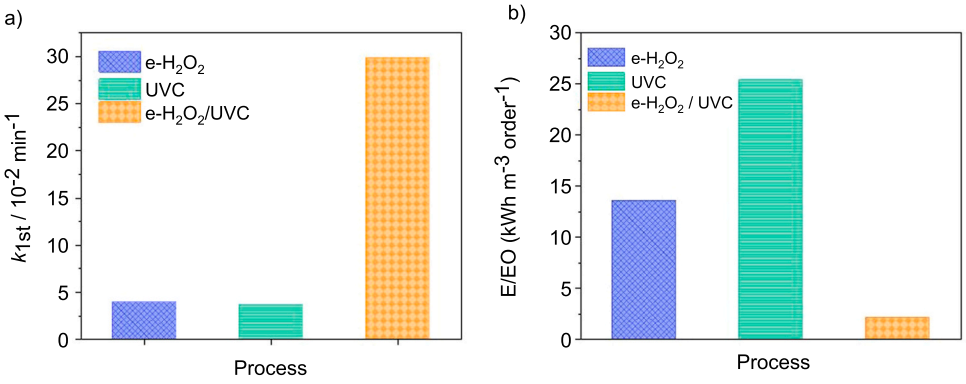

Fig. 6. a) Kinetic rate constant (k_{1st}) values obtained according pseudo-first order model for DEP removal. b) Electrical energy consumed to reduce the concentration of DEP by one order of magnitude under the application of different processes. Current density 50 mA cm^{-2}; UVC lamp (9 W), electrolyte Na_2SO_4 0.5 mol L^{-1}, 1 L, flow rate 250 mL min^{-1}, pH 2.5, duration: 90 min.

Table 1
Information on the molecular ion, fragments and retention time of DEP and its degradation products.

Compound	Retention Time (minutes)	Molecular Ion $[M+H]^+$	Fragments (*m/z*)
Diethyl phthalate (DEP)	4.51	223	177
DP1	3.70	479	312, 271, 222, 185, 83 and 59
DP2	0.73	495	443, 375, 301, 233, 206, 165 and 105
DP3	0.69	499	431, 363, 295, 227, 159 and 105
DP4	1.42	391	279, 235, 199, 183 and 83
DP5	2.93	353	279, 222, 183, 83 and 59
DP6	3.26	339	284, 183, 83 and 59
DP7	11.31	253	225, 201, 101, 83 and 60
DP8	6.15	271	242, 145, 83 and 59
DP9	4.11	301	279, 222, 83 and 59
DP10	4.56	317	279, 222, 185, 83 and 59
DP11	6.96	227	159, 132, 105 and 64
DP12	2.77	279	264, 235, 222, 183, 145, 83 and 59
DP13	9.60	195	181, 135, 83 and 59
DP14	2.56	165	135, 105 and 64
DP15	9.52	183	159, 83 and 59

subsequent hydroxylation of DP14 generated DP15 with *m/z* 183. This pathway also includes the aromatic ring opening and the generation of short chain carboxylic acids as previously reported in the literature (Jung et al., 2010). Then, e-H_2O_2/UVC process stands out as the most efficient technique since led to more transformations of the DEP to lower molecular weight by-products (formation of dimeric by-products are avoided).

Hydroxylation (Jung et al., 2010; Mansouri et al., 2019; Zhang et al., 2024), demethylation (Peng et al., 2013), dihydroxylation (Peng et al., 2013; Wu et al., 2019), and decarboxylation (Wu et al., 2019; Xu et al., 2007) were the major mechanisms described in the literature involved in DEP degradation, followed by the opening of the aromatic ring (Farissi et al., 2023; Muneer et al., 2001; Xu et al., 2007).

The detection of short-chain carboxylic acids generated after DEP degradation using combined e-H_2O_2/UVC process was carried out to better understand the DEP degradation pathway in this system. As result, acids intermediates detected were oxalic acid (9.4 min), maleic acid (11.5 min), formic acid (14.5 min) and acetic acid (Tr: 15.7 min). As reported in previous studies, oxalic acid was the major recalcitrant oxidized product that remained at high concentrations (66.8 mg L^{-1}) at the end of the treatment, while minor concentrations of maleic acid (0.03 mg L^{-1}), formic acid (1.5 mg L^{-1}) and acetic acid (3.3 mg L^{-1}) were detected. These three acids (maleic, acetic and formic) are formed by ring opening of the aromatic ring of DEP (Bensalah et al., 2019).

4. Conclusions

The utilization of a new electrochemical cell with tangential flow ~~and~~ in the degradation of diethyl phthalate using a novel GDE PL6C/BTDA 2 % for H_2O_2 electrogeneration were comprehensively documented in this work. The results obtained allow to draw the following conclusions:

- Higher Faradaic efficiencies (close to 100 %) are obtained using GDE PL6C/BTDA 2 % when operating at current densities of 50 and 100 mA cm^{-2}, where 50 mA cm^{-2} was selected as best choice due to the lower energy consumption. Higher current densities (>100 mA cm^{-2}) promotes the reduction of oxygen to water, causing an important decrease in current efficiency for both GDEs studied.
- Among EAOPs employed to evaluate DEP degradation, the combined e-H_2O_2/UVC system yielded the most favorable results leading to the complete degradation of DEP within 30 minutes of treatment at the lowest energy cost compared to the other process studied. The outstanding performance can be associated to the electro-activation of BTDA and generation of hydroxyl radicals (•OH) through the activation of H_2O_2 by UVC light, which is more effective in the elimination of DEP than single photolysis and treatment with H_2O_2 electrogenerated.
- The proposed degradation pathway revealed that in the e-H_2O_2/UVC process, the aromatic ring opens, and short-chain carboxylic acids are generated. This process facilitates the transformation of DEP into lower molecular weight by-products and prevents the formation of dimeric by-products detected in single photolysis.
- The findings presented in this study underscore the significance of the synergistic combination of an exceptional divided cell, catalytic material and an electrochemical cell featuring tangential flow, rendering the technology viable for practical implementation for the remarkable performance in terms of current efficiency. Also, as future perspective opens the possibility of integration of anodic and cathodic process in the development of a new generation of cells capable of treating simultaneously two wastes in both compartments of the cell.

CRediT authorship contribution statement

Marcos Roberto de R. V. Lanza: Writing – review & editing, Supervision, Funding acquisition, Conceptualization. **Renata Colombo:**

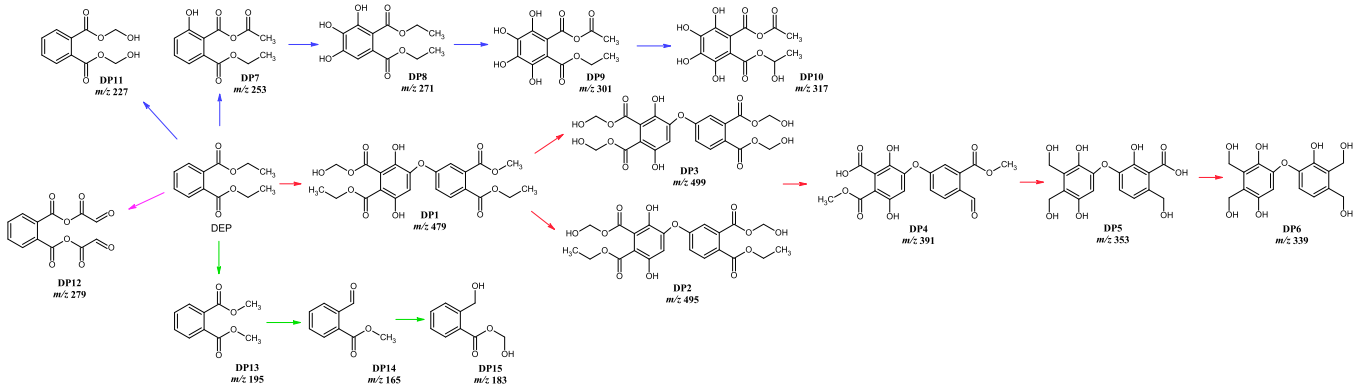

Fig. 7. Proposed degradation pathways of DEP using different advanced oxidation processes. Pathway I (⟶), Pathway II (⟶), Pathway III (⟶) Pathway IV (⟶).

Writing – review & editing, Formal analysis. **Manuel Andres Rodrigo:** Writing – review & editing, Supervision, Funding acquisition, Conceptualization. **Gessica O. S. Santos:** Writing – original draft, Methodology, Formal analysis, Conceptualization. **Taynara Oliveira Silva:** Writing – original draft, Methodology, Formal analysis, Conceptualization.

Declaration of Competing Interest

The authors declare that they have no known competing financial interests or personal relationships that could have appeared to influence the work reported in this paper.

Acknowledgements

The authors acknowledge the funding received by the Brazilian funding agencies including the Brazilian National Council for Scientific and Technological Development (CNPq – grant #303943/2021-1) and São Paulo Research Foundation (FAPESP – grant #2019/08701-4; #2022/07227-0; #2020/02743-4; #2022/03386-6; #2017/10118-0). This work is part of the research project PID2022–138401OB-I00 funded by MCIN/AEI/ and "Unión Europea Next Generation EU/PRTR.

Appendix A. Supporting information

Supplementary data associated with this article can be found in the online version at doi:10.1016/j.psep.2024.05.092.

References

Adinaveen, T., Kennedy, L.J., Vijaya, J.J., Sekaran, G., 2013. Studies on structural, morphological, electrical and electrochemical properties of activated carbon prepared from sugarcane bagasse. J. Ind. Eng. Chem. 19, 1470–1476. https://doi.org/10.1016/j.jiec.2013.01.010.

Barros, W.R.P., Ereno, T., Tavares, A.C., Lanza, M.R.V., 2015. In situ electrochemical generation of hydrogen peroxide in alkaline aqueous solution by using an unmodified gas diffusion electrode. ChemElectroChem 2, 714–719. https://doi.org/10.1002/celc.201402426.

Bensalah, N., Dbira, S., Bedoui, A., 2019. Environmental nanotechnology, monitoring & management mechanistic and kinetic studies of the degradation of diethyl phthalate (DEP) by homogeneous and heterogeneous Fenton oxidation. Environ. Nanotechnol. Monit. Manag. 11, 100224 https://doi.org/10.1016/j.enmm.2019.100224.

Brillas, E., 2014. A review on the degradation of organic pollutants in waters by UV photoelectro-fenton and solar photoelectro-fenton. J. Braz. Chem. Soc. 25, 393–417. https://doi.org/10.5935/0103-5053.20130257.

Bu, Y., Wang, Y., Han, G., Zhao, Y., Ge, X., Li, F., Zhang, Z., Zhong, Q., Baek, J., 2022. Carbon-based electrocatalysts for efficient hydrogen peroxide production. Adv. Mater. 2103266, 1–19. https://doi.org/10.1002/adma.202103266.

Carneiro, J.F., Trevelin, L.C., Lima, A.S., Meloni, G.N., Bertotti, M., Hammer, P., Bertazzoli, R., Lanza, M.R.V., 2017. Synthesis and characterization of ZrO2/C as electrocatalyst for oxygen reduction to H2O2. Electrocatalysis 8, 189–195. https://doi.org/10.1007/s12678-017-0355-0.

Chai, X.S., Hou, Q.X., Luo, Q., Zhu, J.Y., 2004. Rapid determination of hydrogen peroxide in the wood pulp bleaching streams by a dual-wavelength spectroscopic method. Anal. Chim. Acta 507, 281–284. https://doi.org/10.1016/j.aca.2003.11.036.

Chaplin, B.P., 2014. Critical review of electrochemical advanced oxidation processes for water treatment applications. Environ. Sci. Process. Impacts 16, 1182–1203. https://doi.org/10.1039/c3em00679d.

Chingin, K., Chen, H., Gamez, G., Zhu, L., Zenobi, R., Zu, C.-, 2009. Detection of diethyl phthalate in perfumes by extractive electrospray ionization mass. Anal. Chem. 81, 123–129. https://doi.org/10.1039/B818541G.(63).

Cordeiro-Junior, P.J.M., Gonçalves, R., Guaraldo, T.T., da Silva Paiva, R., Pereira, E.C., Lanza, M.R. de V., 2020a. Oxygen reduction reaction: semi-empirical quantum mechanical and electrochemical study of Printex L6 carbon black. Carbon N. Y 156, 1–9. https://doi.org/10.1016/j.carbon.2019.09.036.

Cordeiro-Junior, P.J.M., Kronka, M.S., Goulart, L.A., Veríssimo, N.C., Mascaro, L.H., Santos, M.C. dos, Bertazzoli, R., Lanza, M.R. de V., 2020b. Catalysis of oxygen reduction reaction for H2O2 electrogeneration: the impact of different conductive carbon matrices and their physicochemical properties. J. Catal. 392, 56–68. https://doi.org/10.1016/j.jcat.2020.09.020.

Cordeiro-Junior, P.J.M., Lobato Bajo, J., Lanza, M.R.D.V., Rodrigo Rodrigo, M.A., 2022a. Highly efficient electrochemical production of hydrogen peroxide using the GDE technology. Ind. Eng. Chem. Res. 61, 10660–10669. https://doi.org/10.1021/acs.iecr.2c01669.

Cordeiro-Junior, P.J.M., Martins, A.S., Pereira, G.B.S., Rocha, F.V., Rodrigo, M.A.R., Lanza, M.R. de V., 2022b. Bisphenol-S removal via photoelectro-fenton/H2O2 process using Co-porphyrin/Printex L6 gas diffusion electrode. Sep. Purif. Technol. 285 https://doi.org/10.1016/j.seppur.2021.120299.

da Costa, A.J.M., Kronka, M.S., Cordeiro-Junior, P.J.M., Fortunato, G.V., dos Santos, A.J., Lanza, M.R.V., 2021. Treatment of Tebuthiuron in synthetic and real wastewater using electrochemical flow-by reactor. J. Electroanal. Chem. 882, 114978 https://doi.org/10.1016/j.jelechem.2021.114978.

da Silva, L.M., Mena, I.F., Montiel, M.A., Saez, C., Motheo, A.J., Rodrigo, M.A., 2023. Results in engineering electrochemical generation of ozone for application in environmental remediation. Results Eng. 20, 101436 https://doi.org/10.1016/j.rineng.2023.101436.

De Araújo, K.S., Antonelli, R., Gaydeczka, B., Granato, A.C., Malpass, G.R.P., 2016. Advanced oxidation processes: a review regarding the fundamentals and applications in wastewater treatment and industrial wastewater. Ambient. e Agua - Interdiscip. J. Appl. Sci. 11, 387. https://doi.org/10.4136/ambi-agua.1862.

Dong, C.Di, Chen, T.S., Chen, C.W., Huang, K.L., 2016. Electrochemical degradation of diethyl phthalate under different operating conditions. Int. J. Electrochem. Sci. 11, 5009–5020. https://doi.org/10.20964/2016.06.77.

Escobar, E.A., Zapata, M.Á.V., Hernández, S.A., Valle, S.O.F., Berny, O.R., Ángeles, V.J.G., Reyes, I.C., 2010. Photocatalytic reduction of benzophenone on TiO2: effect of preparation method and reaction conditions. J. Mex. Chem. Soc. 54, 133–138.

Farissi, S., Ramesh, S., Gado, A.A., Tejomurtula, P., Muthukumar, A., Muthuchamy, M., 2023. Electrochemical oxidation of diethyl phthalate at two dimensional graphite sheet electrodes: optimization and analysis of degradation in water with HRMS. J. Appl. Electrochem. 53, 1389–1403. https://doi.org/10.1007/s10800-023-01860-9.

Fromme, H., Küchler, T., Otto, T., Pilz, K., Müller, J., Wenzel, A., 2002. Occurrence of phthalates and bisphenol A and F in the environment. Water Res. 36, 1429–1438. https://doi.org/10.1016/S0043-1354(01)00367-0.

Giomo, M., Buso, A., Fier, P., Sandonà, G., Boye, B., Farnia, G., 2008. A small-scale pilot plant using an oxygen-reducing gas-diffusion electrode for hydrogen peroxide electrosynthesis. Electrochim. Acta 54, 808–815. https://doi.org/10.1016/j.electacta.2008.06.038.

Heudorf, U., Mersch-Sundermann, V., Angerer, J., 2007. Phthalates: toxicology and exposure. Int. J. Hyg. Environ. Health 210, 623–634. https://doi.org/10.1016/j.ijheh.2007.07.011.

Hong, J., Moon, H., Kim, J., Lee, B., Kim, G., Lee, H., Kim, Y., 2021. Chemosphere differentiation of carbon black from black carbon using a ternary plot based on elemental analysis. Chemosphere 264, 128511. https://doi.org/10.1016/j.chemosphere.2020.128511.

Hou, A., Sun, G., 2013. Multifunctional finishing of cotton fabrics with 3,3′,4,4′-benzophenone tetracarboxylic dianhydride: reaction mechanism. Carbohydr. Polym. 95, 768–772. https://doi.org/10.1016/j.carbpol.2013.02.027.

Jing, Y., Chaplin, B.P., 2017. Mechanistic study of the validity of using hydroxyl radical probes to characterize electrochemical advanced oxidation processes. Environ. Sci. Technol. 51, 2355–2365. https://doi.org/10.1021/acs.est.6b05513.

Jung, Y.J., Oh, B.S., Kim, K.S., Koga, M., Shinohara, R., Kang, J., 2010. The degradation of diethyl phthalate (DEP) during ozonation: oxidation by-products study. J. Water Health 8, 290–298. https://doi.org/10.2166/wh.2009.301.

Kronka, M.S., Fortunato, G.V., Mira, L., dos Santos, A.J., Lanza, M.R.V., 2023. Using Au NPs anchored on ZrO2/carbon black toward more efficient H2O2 electrogeneration in flow-by reactor for carbaryl removal in real wastewater. Chem. Eng. J. 452, 139598 https://doi.org/10.1016/j.cej.2022.139598.

Kulkarni, A., Siahrostami, S., Patel, A., Nørskov, J.K., 2018. Understanding catalytic activity trends in the oxygen reduction reaction. Chem. Rev. 118, 2302–2312. https://doi.org/10.1021/acs.chemrev.7b00488.

Li, W., Jain, T., Ishida, K., Liu, H., 2017. A mechanistic understanding of the degradation of trace organic contaminants by UV/hydrogen peroxide, UV/persulfate and UV/free chlorine for water reuse. Environ. Sci. Water Res. Technol. 3, 128–138. https://doi.org/10.1039/c6ew00242k.

Lima, V.B., Goulart, L.A., Rocha, R.S., Steter, J.R., Lanza, M.R.V., 2020. Degradation of antibiotic ciprofloxacin by different AOP systems using electrochemically generated hydrogen peroxide. Chemosphere 247, 125807. https://doi.org/10.1016/j.chemosphere.2019.125807.

Ma, R., Lin, G., Zhou, Y., Liu, Q., Zhang, T., Shan, G., Yang, M., Wang, J., 2019. A review of oxygen reduction mechanisms for metal-free carbon-based electrocatalysts. NPJ Comput. Mater. 5 https://doi.org/10.1038/s41524-019-0210-3.

Mansouri, L., Tizaoui, C., Geissen, S., Bousselmi, L., 2019. A comparative study on ozone, hydrogen peroxide and UV based advanced oxidation processes for efficient removal of diethyl phthalate in water. J. Hazard. Mater. 363, 401–411. https://doi.org/10.1016/j.jhazmat.2018.10.003.

Marques Cordeiro-Junior, P.J., Sáez Jiménez, C., Vasconcelos Lanza, M.R. de, Rodrigo Rodrigo, M.A., 2022. Electrochemical production of extremely high concentrations of hydrogen peroxide in discontinuous processes. Sep. Purif. Technol. 300 https://doi.org/10.1016/j.seppur.2022.121847.

Medellin-Castillo, N.A., Ocampo-Pérez, R., Leyva-Ramos, R., Sanchez-Polo, M., Rivera-Utrilla, J., Méndez-Díaz, J.D., 2013. Removal of diethyl phthalate from water solution by adsorption, photo-oxidation, ozonation and advanced oxidation process (UV/H2O2, O3/H2O2 and O3/activated carbon). Sci. Total Environ. 442, 26–35. https://doi.org/10.1016/j.scitotenv.2012.10.062.

Michielli, R.F., Elving, P.J., 1968. Electrochemical reduction of benzophenone in aprotic medium. Effect of proton availability. J. Am. Chem. Soc. 90, 1989–1995. https://doi.org/10.1021/ja01010a011.

Moratalla, Á., Araújo, D.M., Moura, G.O.M.A., Lacasa, E., Cañizares, P., Rodrigo, M.A., Sáez, C., 2021. Pressurized electro-Fenton for the reduction of the environmental impact of antibiotics. Sep. Purif. Technol. 276 https://doi.org/10.1016/j.seppur.2021.119398.

Moreira, J., Bocalon Lima, V., Athie Goulart, L., Lanza, M.R.V., 2019. Electrosynthesis of hydrogen peroxide using modified gas diffusion electrodes (MGDE) for environmental applications: Quinones and azo compounds employed as redox modifiers. Appl. Catal. B Environ. 248, 95–107. https://doi.org/10.1016/j.apcatb.2019.01.071.

Muneer, M., Theurich, J., Bahnemann, D., 2001. Titanium dioxide mediated photocatalytic degradation of 1, 2-diethyl phthalate. J. Photochem. Photobiol. A Chem. 143, 213–219.

Oturan, M.A., Aaron, J.J., 2014. Advanced oxidation processes in water/wastewater treatment: principles and applications. A review. Crit. Rev. Environ. Sci. Technol. 44, 2577–2641. https://doi.org/10.1080/10643389.2013.829765.

Peng, X., Feng, L., Li, X., 2013. Chemosphere Pathway of diethyl phthalate photolysis in sea-water determined by gas chromatography – mass spectrometry and compound-specific isotope analysis. Chemosphere 90, 220–226. https://doi.org/10.1016/j.chemosphere.2012.06.045.

Posher, R.A., 1983. Functional groups in carbon black by ftir spectroscopy. Carbon N. Y 21, 47–51.

Quan, Y., Liu, Q., Zhang, Shilong, Zhang, Shuai, 2018. Applied Surface Science Comparison of the morphology, chemical composition and microstructure of cryptocrystalline graphite and carbon black. Appl. Surf. Sci. 445, 335–341. https://doi.org/10.1016/j.apsusc.2018.03.182.

Sánchez-Montes, I., Santos, O.S., G, Silva, O., Colombo, T., R, R. V. Lanza, M., 2023. An innovative approach to the application of electrochemical processes based on the in-situ generation of H2O2 for water treatment. J. Clean. Prod. 392 https://doi.org/10.1016/j.jclepro.2023.136242.

Silva, T.O., Goulart, A., Sánchez-Montes, L., I, Santos, O.S., G, B. Santos, R., Colombo, R., R. V. Lanza, M., 2022. Using a novel gas diffusion electrode based on PL6 carbon modified with benzophenone for efficient H2O2 electrogeneration and degradation of ciprofloxacin. Chem. Eng. J. 455, 140697 https://doi.org/10.1016/j.cej.2022.140697.

Silva, T.O., Fernandez-Cascán, J., Isidro, J., Saez, C., Marcos, M.R., Rodrigo, M.A., 2023. Degradation of real lindane wastes using advanced oxidation technologies based on electrogenerated hydrogen peroxide. Process Saf. Environ. Prot. 180, 535–543. https://doi.org/10.1016/j.psep.2023.10.031.

Song, C., Wang, L., Ren, J., Lv, B., Sun, Z., Yan, J., Li, X., Liu, J., 2016. Comparative study of diethyl phthalate degradation by UV/H2O2 and UV/TiO2: kinetics, mechanism, and effects of operational parameters. Environ. Sci. Pollut. Res. 23, 2640–2650. https://doi.org/10.1007/s11356-015-5481-8.

Song, Y., Cui, C., Liu, Y., 2016. Journal of photochemistry and photobiology A: chemistry theoretical study of the homolytic photolysis of hydrogen peroxide at the state-of-the-art level. J. Photochem. Photobiol. A Chem. 317, 68–71. https://doi.org/10.1016/j.jphotochem.2015.11.014.

Muddemann, Thorben, Haupt, Dennis R., Sievers, Michael, U.K, 2020. Improved operating parameters for hydrogen peroxide-generating gas diffusion electrodes. Chem. Ing. Tech. 92, 505–512. https://doi.org/10.1002/cite.201900137.

Valim, R.B., Trevelin, L.C., Sperandio, D.C., Carneiro, J.F., Santos, M.C., Rodrigues, L.A., Rocha, R.S., Lanza, M.R.V., 2021. Using carbon black modified with Nb2O5 and RuO2 for enhancing selectivity toward H2O2 electrogeneration. J. Environ. Chem. Eng. 9, 106787 https://doi.org/10.1016/j.jece.2021.106787.

Van Wezel, A.P., Van Vlaardingen, P., Posthumus, R., Crommentuijn, G.H., Sijm, D.T.H. M., 2000. Environmental risk limits for two phthalates, with special emphasis on endocrine disruptive properties. Ecotoxicol. Environ. Saf. 46, 305–321. https://doi.org/10.1006/eesa.2000.1930.

Wang, J., Li, C., Rauf, M., Luo, H., Sun, X., Jiang, Y., 2021. Gas diffusion electrodes for H2O2 production and their applications for electrochemical degradation of organic pollutants in water: a review. Sci. Total Environ. 759, 143459 https://doi.org/10.1016/j.scitotenv.2020.143459.

Wang, J.L., Xu, L.E.J.I.N., 2012. Advanced oxidation processes for wastewater treatment: formation of hydroxyl radical and application advanced oxidation processes for wastewater treatment: formation of hydroxyl radical. Environ. Sci. Technol. 3389, 251–325. https://doi.org/10.1080/10643389.2010.507698.

Wu, Y., Deng, L., Bu, L., Zhu, S., Shi, Z., Zhou, S., 2019. Degradation of diethyl phthalate (DEP) by vacuum ultraviolet process: influencing factors, oxidation products, and toxicity assessment. Environ. Sci. Pollut. Res. 5435–5444.

Xia, C., Xia, Y., Zhu, P., Fan, L., 2019. Direct electrosynthesis of pure aqueous H 2 O 2 solutions up to 20% by weight using a solid electrolyte. Science 231 (80-.), 1–5.

Xiao, Q., Ouyang, L., 2009. Photocatalytic activity and hydroxyl radical formation of carbon-doped TiO 2 nanocrystalline: Effect of calcination temperature. Chem. Eng. J. J. 148, 248–253. https://doi.org/10.1016/j.cej.2008.08.024.

Xu, B., Gao, N.Y., Sun, X.F., Xia, S.J., Rui, M., Simonnot, M.O., Causserand, C., Zhao, J.F., 2007. Photochemical degradation of diethyl phthalate with UV/H2O2. J. Hazard. Mater. 139, 132–139. https://doi.org/10.1016/j.jhazmat.2006.06.026.

Yang, G.P., Zhao, X.K., Sun, X.J., Lu, X.L., 2005. Oxidative degradation of diethyl phthalate by photochemically-enhanced Fenton reaction. J. Hazard. Mater. 126, 112–118. https://doi.org/10.1016/j.jhazmat.2005.06.014.

Yegorov, A.S., Wozniak, A.I., Ivanov, V.S., Averina, E.A., Zhdanovich, O.A., 2016. Development and optimization of producing 3,3′, 4,4′-benzophenonetetracarboxylic dianhydride. Orient. J. Chem. 32, 3063–3070. https://doi.org/10.13005/ojc/320627.

Yu, F., Zhou, M., Zhou, L., Peng, R., 2014. A novel electro-fenton process with H2O2 generation in a rotating disk reactor for organic pollutant degradation. Environ. Sci. Technol. Lett. 1, 320–324. https://doi.org/10.1021/ez500178p.

Zhang, S., Wei, J., Wu, N., Allam, A.A., Ajarem, J.S., Maodaa, S., Huo, Z., Zhu, F., Qu, R., 2024. Assessment of the UV / DCCNa and UV / NaClO oxidation process for the removal of diethyl phthalate (DEP) in the aqueous system. Environ. Pollut. 341, 122915 https://doi.org/10.1016/j.envpol.2023.122915.

Zhou, W., Meng, X., Gao, J., Alshawabkeh, A.N., 2019. Hydrogen peroxide generation from O2 electroreduction for environmental remediation: a state-of-the-art review. Chemosphere 225, 588–607. https://doi.org/10.1016/j.chemosphere.2019.03.042.

Zhu, Q., Pan, Z., Hu, S., Kim, J.H., 2019. Cathodic hydrogen peroxide electrosynthesis using anthraquinone modified carbon nitride on gas diffusion electrode. ACS Appl. Energy Mater. 2, 7972–7979. https://doi.org/10.1021/acsaem.9b01445.